

# Study on the Load-bearing Capacity of X80 Submerged Arc Welded Joints Based on Finite Element Model

Zhen Zhang

School of Materials Science and Engineering, Xi'an Shiyou University, Xian 710065, China

**Abstract:** *As the petroleum industry continues to expand rapidly, X80 pipeline steel has become a key material in oil and gas transportation due to its strength and durability. However, welding joints, a critical part of these pipelines, sometimes lack sufficient load-bearing capacity, leading to structural failures. Ensuring the mechanical integrity of these joints is essential for the safe and efficient operation of pipelines. This study employs ABAQUS finite element analysis to assess the performance of welded joints created using submerged arc welding (SAW) and gas metal arc welding (GMAW). By developing 3D models, the study simulates tensile testing, revealing that as displacement increases, the tensile force rises, causing plastic deformation. Necking occurs near the heat-affected zone in the base metal, eventually leading to fracture. Furthermore, internal pressure simulations show that as pressure builds, the highest stress concentration appears on the inner wall of the welded joints, emphasizing the importance of weld strength in high-pressure environments. By visually demonstrating the mechanical behavior of different welding techniques, this study provides valuable insights for improving welding processes in X80 pipeline steel. The findings serve as a theoretical foundation for optimizing pipeline construction and ensuring long-term structural safety in real-world applications.*

**Keywords:** X80 pipeline steel; Welded joints; Load-bearing capacity; Finite element analysis.

## 1. INTRODUCTION

Studies indicate that X80 pipelines have been extensively employed in the transmission of oil and natural gas. China is not only a major consumer of X80 pipelines but also the world's largest producer. The total installed length of X80 pipelines in various countries exceeds 8000 km, with widespread application in numerous engineering projects [1-4]. Among the critical concerns in the petroleum pipeline industry, the load-bearing capacity of X80 pipeline steel during service, particularly experimental investigations related to this aspect, has garnered significant attention [5-7].

Turichin et al. [8] investigated the effects of different welding processes on the hardness and tensile strength of X80 welded pipes. Xie Zhiyuan et al. [9] analyzed the fatigue behavior of the heat-affected zone (HAZ) in welded joints of X80 strain-based design (SBD) pipelines. Their findings revealed a significant reduction in fatigue performance in the HAZ, with the weld toe identified as the primary initiation site for fatigue cracks. Midawi et al. [10] conducted a comparative study on the microstructural morphology, tensile properties, and hardness of two welding electrodes used in X80 pipeline welding. The results demonstrated that welding consumables with higher alloying content enhanced weld strength, whereas those with lower alloying content improved weld toughness.

Sousa et al. [21] examined the mechanical properties and residual stress distribution of welded joints fabricated using two different welding techniques. The findings indicated that residual stress was the predominant type of stress present in the welded joints, regardless of the welding method. Kim et al. [22] investigated the fatigue crack propagation behavior in high-strength X80 pipelines, revealing distinct differences in crack propagation characteristics among the HAZ, weld metal, and base metal. Additionally, the fatigue life of welded joints was observed to be prolonged compared to that of X80 pipeline base material.

Chen et al. [24] employed finite element analysis (FEA) software to simulate the mechanical behavior of three different X80 pipeline steels, focusing on the influence of chemical composition and welding parameters on the HAZ's mechanical properties and microstructure. The results indicated that an increase in cooling rate led to a significant refinement of the low-temperature microstructure, enhancing both the strength and toughness of the welded joints.

In conclusion, this study focuses on key factors influencing the load-bearing capacity of welded joints. Finite element simulations were conducted to analyze the internal pressure and tensile load-bearing capacity of

submerged arc welded (SAW) and gas metal arc welded (GMAW) joints. The findings aim to provide optimized welding procedures and process parameters for X80 pipeline steel applications.

## 2. RESEARCH METHODOLOGY

### 2.1 Experimental Principle

The ABAQUS finite element software was utilized to simulate and analyze the welded joints of X80 pipeline steel fabricated by submerged arc welding (SAW) and gas metal arc welding (GMAW). In the tensile simulation, a fixed constraint was applied to one end while a tensile load was imposed on the other to evaluate the mechanical response of the joint. The obtained results were used to generate load-displacement curves for further analysis. For the internal pressure simulation, a shell model was employed, with internal pressure applied to the inner wall to assess the load-bearing capacity of the welded joint under internal pressurization. The results were similarly used to construct pressure-deformation curves, providing a basis for further data interpretation and evaluation.

## 3. TENSILE SIMULATION OF X80 PIPELINE STEEL

### 3.1 Processing of Tensile Test Model

In this study, the numerical simulation of the tensile behavior of welded joints was conducted using ABAQUS software. Considering the large dimensions of the actual X80 pipeline, the model was appropriately simplified to enhance computational efficiency and reduce processing time.

Modeling of Submerged Arc Welded (SAW) Joints.

A 3D geometric model was constructed, with a cross-section of the welded joint illustrated. The model dimensions include a length of 500 mm, a wall thickness of 21.4mm, and a pipe diameter of 1219 mm. Next, the welded joint was partitioned, and the weld profile, including the weld bead and heat-affected zone (HAZ), was depicted using an arc on the cross-section. The weld reinforcement height was set to 1.98 mm, as shown in Fig 1.

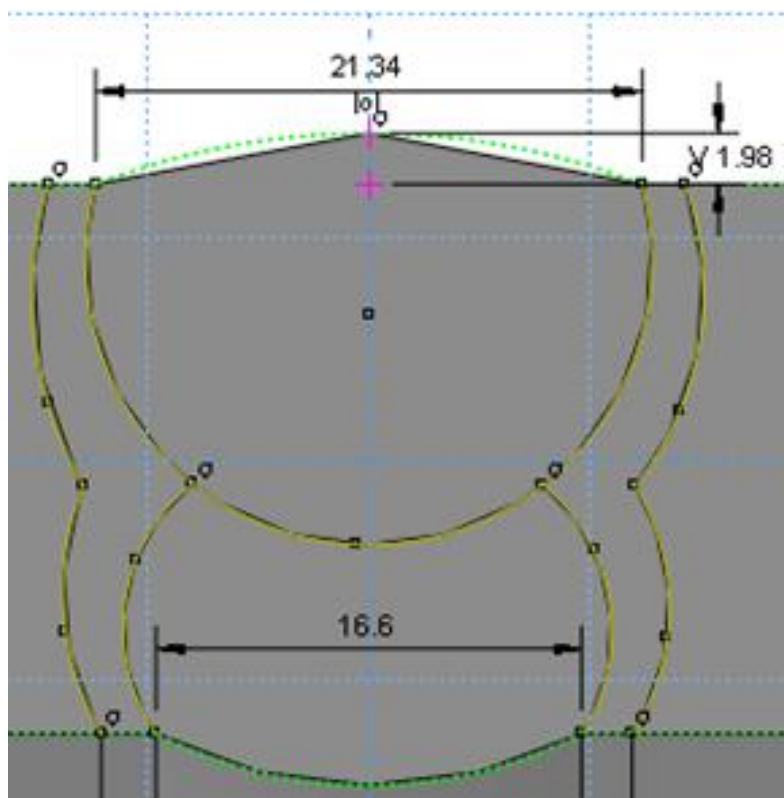


Figure 1: Cross-sectional View of the SAW Joint.

Finally, the sweep operation was performed on the defined weld profile using a partitioning tool. The geometry

was divided into multiple sections, completing the partitioning process, as shown in Figure 2.



**Figure 2:** Geometric Model of the SAW Joint. Modeling of GMAW Joint

A geometric model of the gas metal arc welded (GMAW) joint was established with a length of 500 mm and a thickness of 21.4 mm.

The weld profile was constructed following the previously described method. The weld reinforcement heights were set to 1 mm on the top and 1.8 mm on the bottom, as illustrated in Figure 3, which presents the cross-sectional sketch of the GMAW weld model.

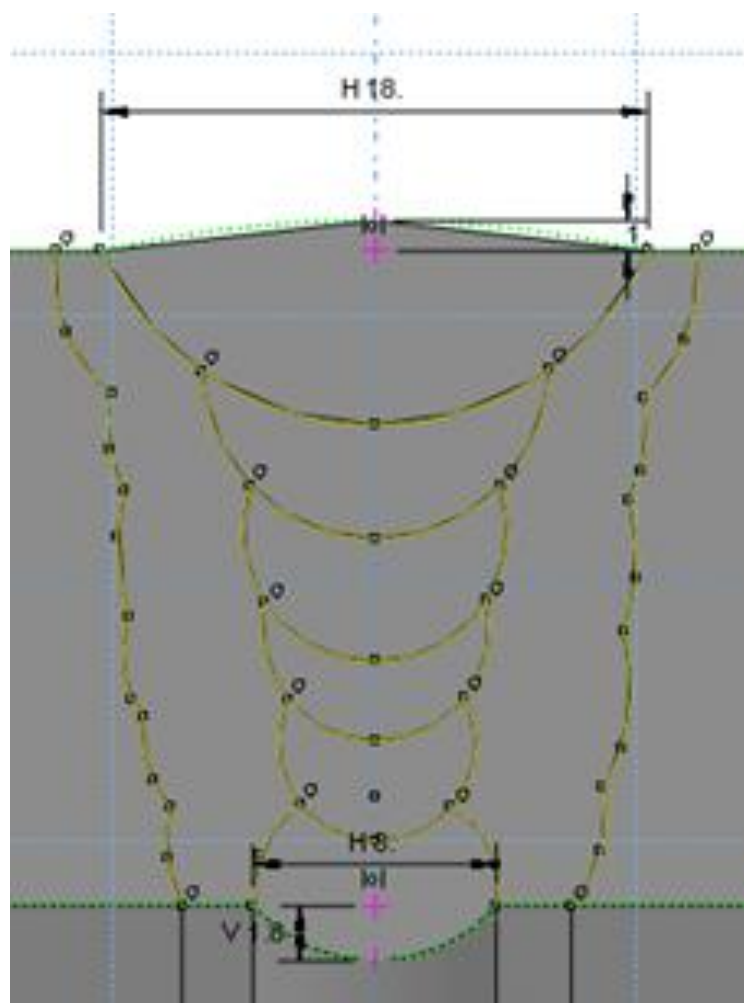


**Figure 3:** which presents the cross-sectional sketch of the GMAW weld model.

The sweep operation was performed as previously described. The geometry was divided into multiple sections to complete the partitioning process, as shown in Figure 4, which illustrates the geometric model of the gas metal arc welded (GMAW) joint.



**Figure 4:** which illustrates the geometric model of the GMAW joint.

### 3.2 Definition of Tensile Test Parameters

#### Definition of Material Properties

In this simulation, tensile testing was conducted, requiring both elastic and plastic material properties. The welded joint models for the two welding methods were divided into three distinct regions: base metal, heat-affected zone (HAZ), and weld metal. Each region was assigned fundamental material parameters, including elasticity and plasticity. The plastic parameters for different regions are detailed in Table 1: Tensile Test Material Properties.

Since the variations in elastic properties among the weld metal, base metal, and HAZ are minimal in the elastic stage, a uniform elastic modulus of 210,000 MPa and a Poisson's ratio of 0.3 were applied. The base metal exhibits relatively high strength, while the strength of the filler material is generally equal to or slightly higher than that of the base metal. In contrast, the HAZ may undergo softening, resulting in lower strength but improved plasticity.

**Table 1:** Tensile Test Material Properties

	Yield Strength/Mpa	Plastic Deformation
Base Metal Plasticity	640	0
	760	0.05
Weld Metal Plasticity	640	0
	760	0.05
Heat-Affected Zone (HAZ) Plasticity	540	0
	660	0.15

#### Analysis Step

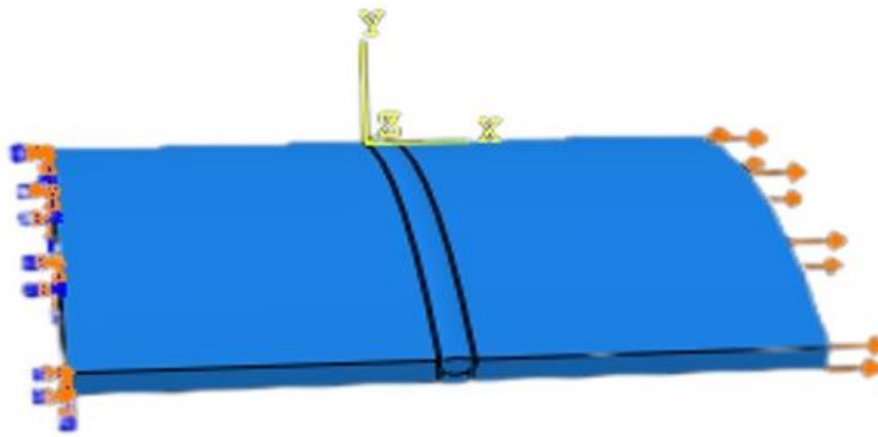
The analysis primarily involved static calculations. Therefore, a static analysis step and a general analysis step were created for both models, with a total simulation time of 10 seconds.

Based on the experimental requirements, the necessary output parameters were selected in the field output settings. The primary output parameters included stress (S), displacement (U), and equivalent plastic strain (PEEQ).

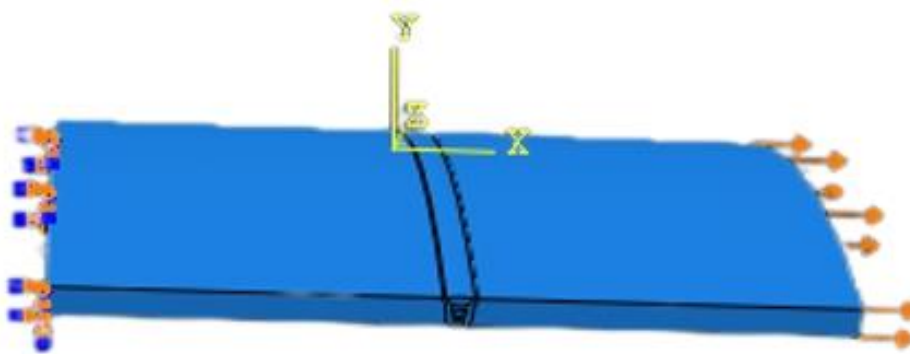
#### Load Application

For the tensile test simulation, one side was fully constrained, while the other was subjected to axial tensile displacement. Boundary constraints were defined in the initial step, and the tensile displacement load was applied during the analysis step.

As illustrated in Figure 5(a) for the submerged arc welding (SAW) model and Figure 5(b) for the gas metal arc welding (GMAW) model, the constraints were implemented accordingly.



(a): for the SAW model



(b): for the GMAW model

**Figure 5: Model Constraints**

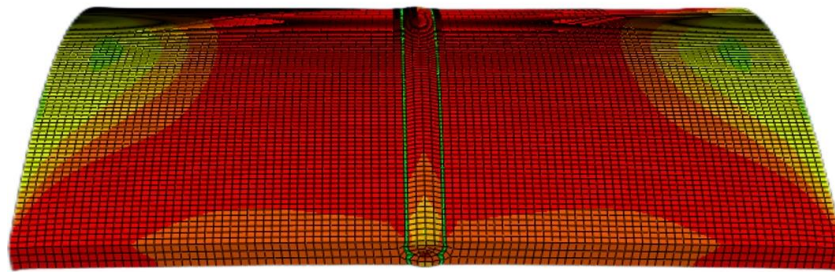
In the designated coordinate system, U1 corresponds to the X-axis, U2 to the Y-axis, and U3 to the Z-axis. The tensile direction was set along the positive X-axis. U1 was selected, and a displacement value of 100 mm was assigned, based on the modeling unit. This configuration applies a 100 mm tensile displacement in the X-axis direction, with a linearly increasing magnitude.

### Mesh Generation

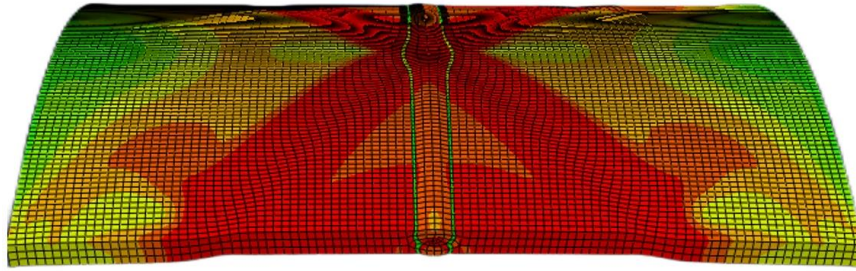
For this simulation, the mesh was generated using a global seeding method. To enhance the accuracy of the numerical results, the global seed size was set to 1 mm. The element type was specified as a 3D stress element, while all other parameters remained at their default settings.

### 3.3 Analysis of Tensile Test Results

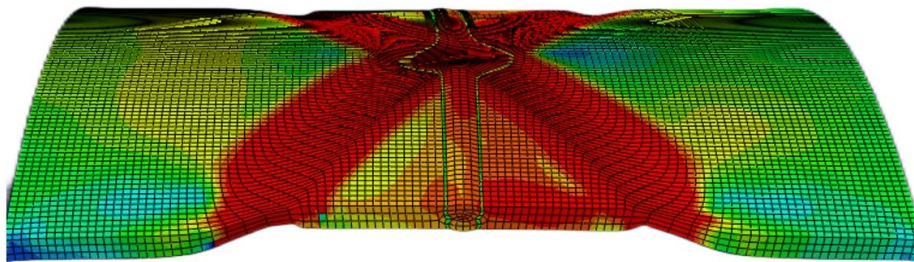
The tensile simulation process for submerged arc welding (SAW) is illustrated in Figure 6. The previously defined field output variables were selected to examine the corresponding results. By adjusting the frame selector, the stress distribution at different time steps was observed. As the applied tensile load increased, the von Mises stress gradually rose within the specimen. Significant deformation occurred in the base metal near the heat-affected zone (HAZ). With further loading, the stress in this region reached its tensile strength, leading to necking initiation.



(a): Tensile Simulation Process of SAW 1



(b): Tensile Simulation Process of SAW 2



(c): Tensile Simulation Process of SAW 3

**Figure 6:** Tensile Stress Contour of SAW

The relationship between tensile force and displacement is shown in Figure 7. As indicated in the graph, when the displacement reaches 25.4918 mm, the tensile force attains its peak. Subsequently, necking occurs in the specimen.

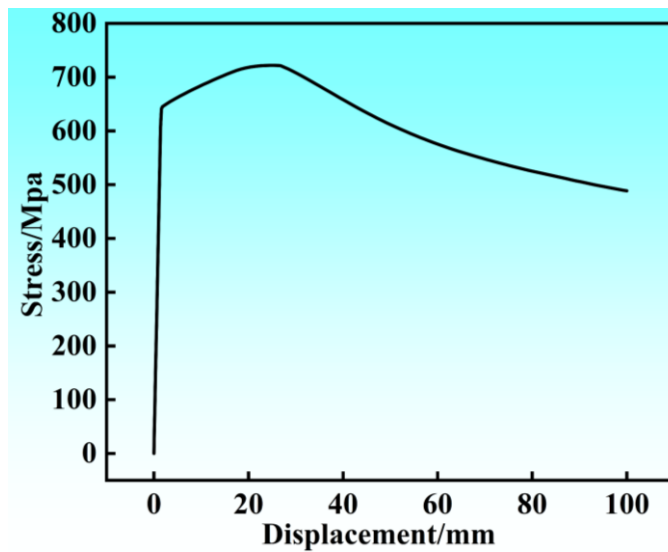
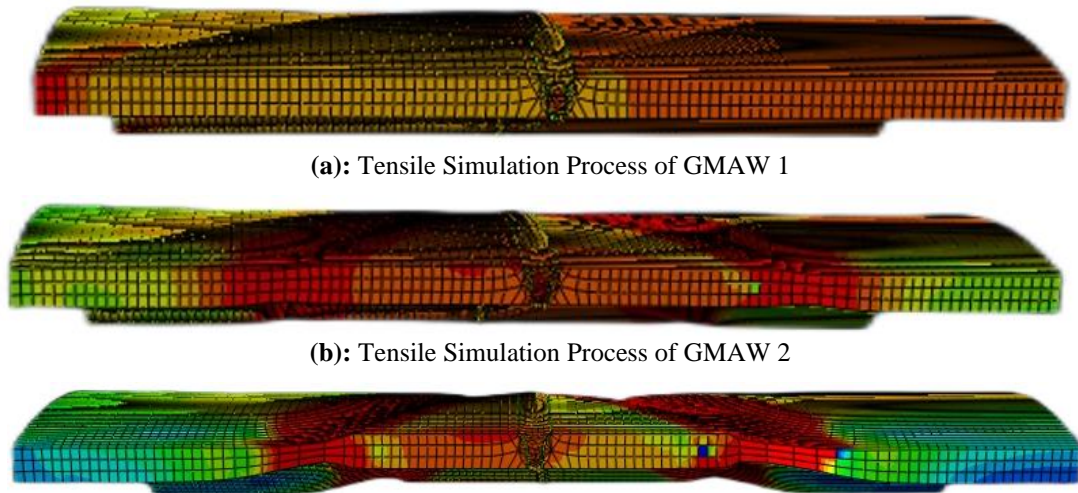


**Figure 7:** Tensile Force-Displacement Curve of the SAW Model

The tensile simulation process for the gas metal arc welded (GMAW) joint is shown in Figure 8. The previously defined field output parameters were selected to analyze the results. As the tensile load increased, the von Mises

stress gradually rose within the specimen. Significant deformation occurred in the base metal near the heat-affected zone (HAZ). With further loading, the stress in this region reached its tensile strength, initiating necking in the specimen.



(a): Tensile Simulation Process of GMAW 1

(b): Tensile Simulation Process of GMAW 2

(c): Tensile Simulation Process of GMAW 3

Figure 7: Tensile Stress Contour of GMAW

The relationship between tensile force and displacement is shown in Figure 8. As indicated in the graph, the tensile force reaches its peak at a displacement of 24.2313 mm. Afterward, necking occurs in the specimen.

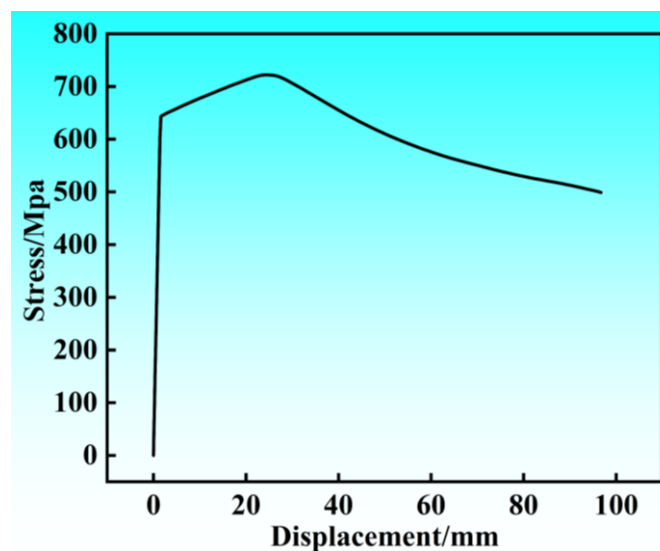


Figure 8: Tensile Force-Displacement Curve of GMAW

## 4. SIMULATION OF INTERNAL PRESSURE TESTS FOR SUBMERGED ARC WELDING AND GAS METAL ARC WELDING OF X80 PIPELINE STEEL

### 4.1 Internal Pressure Test Model

For this internal pressure simulation, an axisymmetric model was established to meet the experimental requirements. The model was defined as a shell with no thickness. The cross-section of the submerged arc welded (SAW) joint is shown in Figure 9. The sketch was created on one side of the central axis, with a radial distance of 609.5 mm, corresponding to the pipeline's radius. The cross-sectional model was then partitioned, with a length of 50 mm and a weld reinforcement height of 1.5mm. The gas metal arc welded (GMAW) joint cross-section is illustrated in Figure 10. Similar to the SAW model, the sketch was drawn on one side of the central axis, maintaining a radius of 609.5 mm. The cross-sectional model was then segmented, with a length of 50 mm, an outer weld reinforcement height of 1 mm, and an inner weld reinforcement height of 1.8 mm.

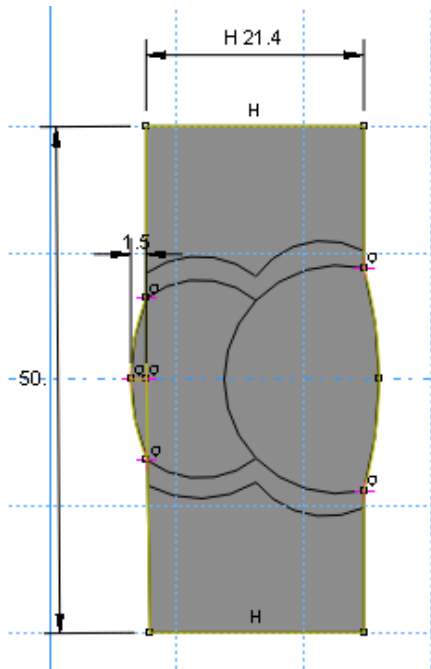


Figure 9: Cross-Section of the SAW Joint

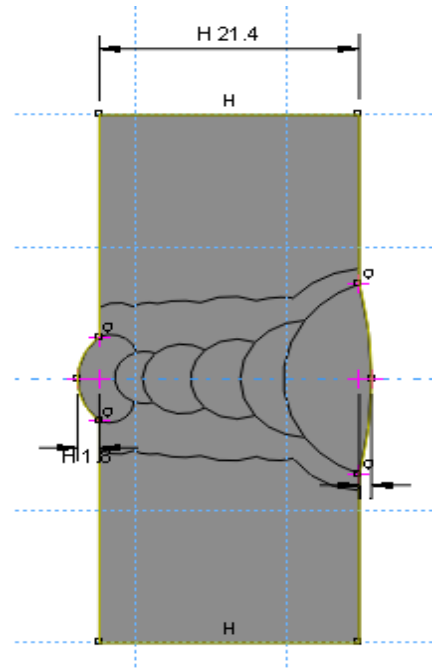


Figure 10: Cross-Section of the GMAW Joint

#### 4.2 Definition of Internal Pressure Test Parameters

##### Definition of Material Properties

Both models were divided into three regions: weld metal, base metal, and heat-affected zone (HAZ). Each region was assigned both elastic and plastic material properties, as detailed in Table 2. Since the variations in elastic properties among the three regions are minimal in the elastic stage, a uniform elastic modulus of 210,000 MPa and a Poisson's ratio of 0.3 were applied

Table 2: Material Properties for Internal Pressure Test

	Yield Strength/Mpa	Plastic Deformation
Base Metal Plasticity	640	0
	760	0.05
Weld Metal Plasticity	640	0
	760	0.05
Heat-Affected Zone (HAZ) Plasticity	540	0
	660	0.15

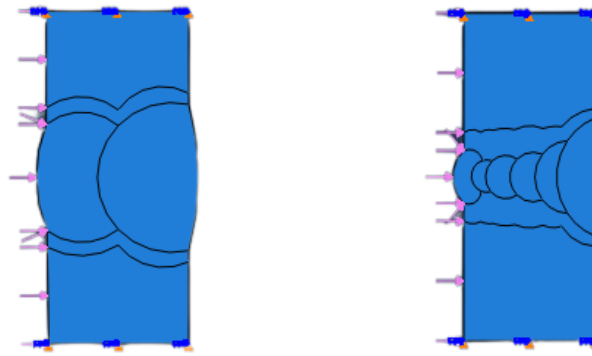
##### Analysis Step

The analysis process for both models focused on static calculations. Therefore, a static general analysis step was established, with a total simulation time of 2 seconds.

##### Load Application

For both models, an internal pressurization load was applied to meet the simulation requirements. The inner wall was selected, and a pressure of 200 MPa was assigned, increasing linearly over time.

Boundary conditions were defined by constraining the displacement of both edges in the Y-direction (axial direction), as illustrated in Figure 11: Internal Pressure Test Load.



(a): Internal Pressure Load for SAW (b): Internal Pressure Load for GMAW  
**Figure 11: Internal Pressure Test Load**

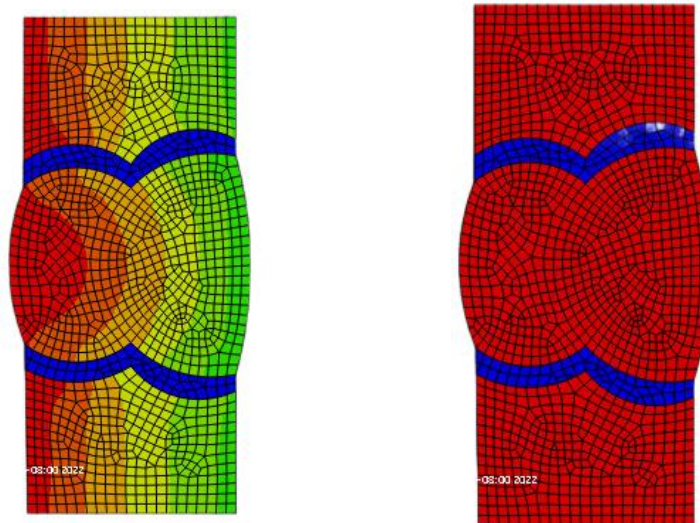
### Mesh Generation

To enhance the accuracy of the simulation results, a global seed size of 1 mm was applied to both models for mesh generation.

### 4.3 Analysis of Internal Pressure Test Results

#### Analysis of SAW Internal Pressure Simulation

The stress contour for the SAW internal pressure test is presented in Figure 12. The total analysis time was 2 seconds, with a maximum applied pressure of 200 MPa. Based on the von Mises stress distribution, at 1.53 seconds, the equivalent stress at the weld location reached 760 MPa, which corresponds to its tensile strength. This moment can be considered as the critical pressure-bearing capacity of the welded joint. The Mises stress curve for the SAW internal pressure test is shown in Figure 13.



(a): Internal Pressure Test Process of 1 (b): Internal Pressure Test Process of 2  
**Figure 12: Stress Contour of Submerged Arc Welding Internal Pressure Test**

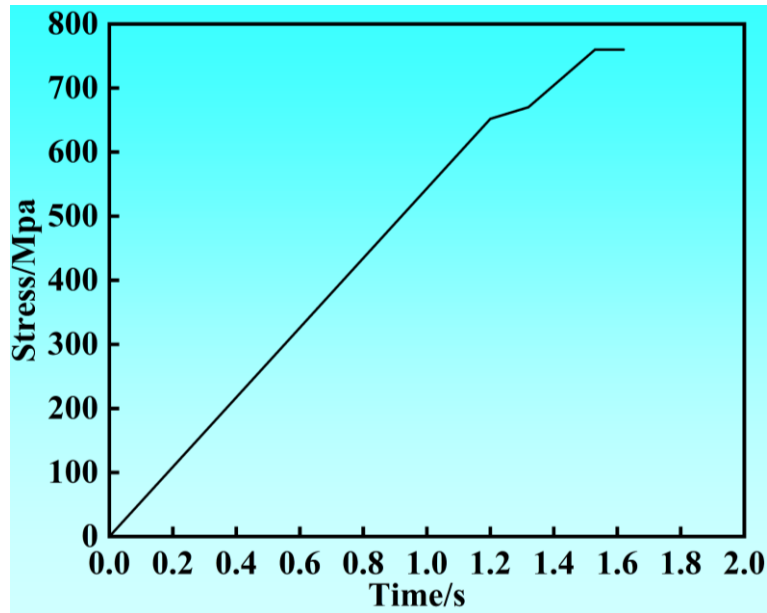


Figure 13: Mises Stress Curve of SAW Internal Pressure Test

#### Analysis of Gas Metal Arc Welding (GMAW) Internal Pressure Simulation

The stress contour for the GMAW internal pressure simulation is shown in Figure 14. The total analysis time was 2 seconds, with a maximum applied pressure of 200 MPa. Based on the von Mises stress distribution, at 0.29 seconds, the equivalent stress at the weld location reached 760 MPa, corresponding to its tensile strength. This moment can be considered as the critical pressure-bearing capacity of the welded joint. The Mises stress curve for the GMAW internal pressure test is illustrated in Figure 15.

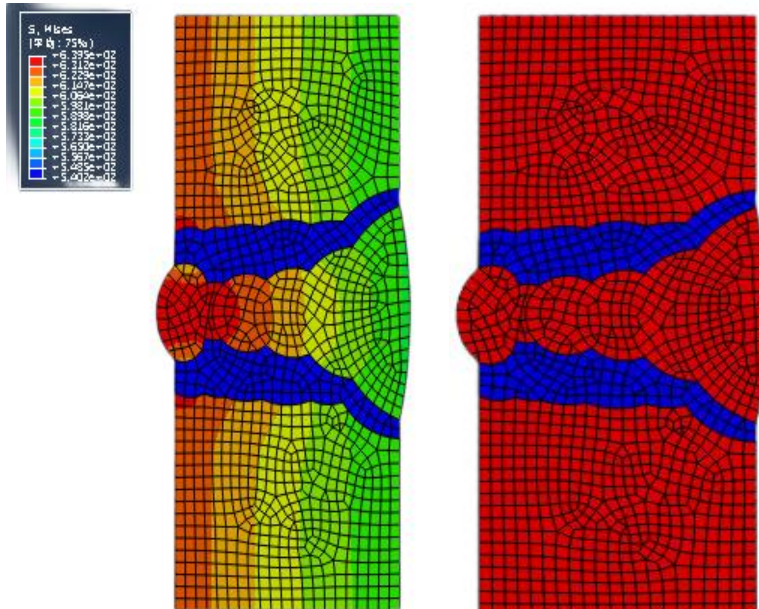


Figure 14: Stress Contour of GMAW Internal Pressure Simulation

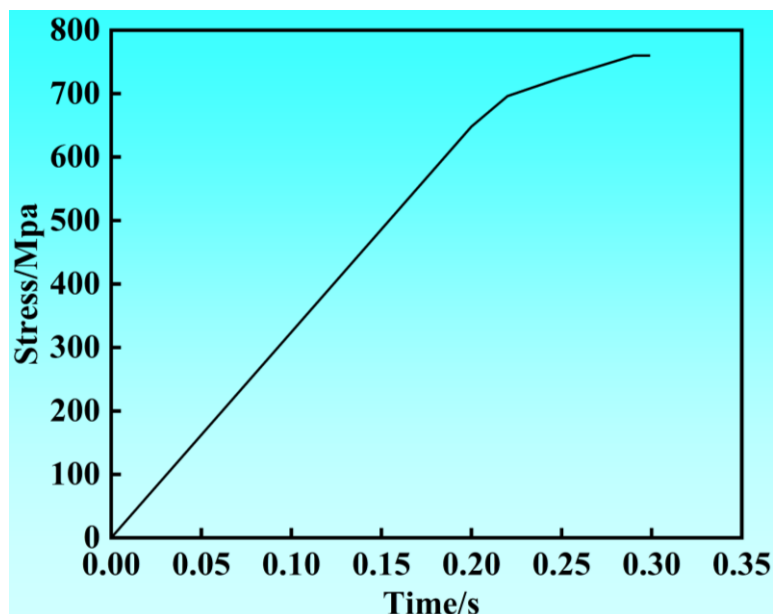


Figure 15: Mises Stress Curve of GMAW Internal Pressure Test

#### 4.4 Summary

Using ABAQUS simulation software, internal pressure load-bearing capacity tests were conducted on submerged arc welded (SAW) joint shell models with a length of 50 mm and a height of 21.4 mm.

The simulation results indicate that during the gradual increase in internal pressure, the welded joint region on the inner wall consistently experienced higher pressure than other areas. Eventually, both types of welded joints reached their tensile strength. Enhancing the compressive strength at the inner wall joint is crucial for improving the overall welded joint quality.

### 5. EXPERIMENTAL CONCLUSIONS

Through on-site welding investigations and a review of relevant literature, several key factors affecting the load-bearing capacity of welded joints in practical engineering applications were identified. These factors were categorized into four major aspects: material properties, environmental conditions, structural characteristics, and welding processes, with corresponding explanations provided.

Finite element tensile simulations were conducted on submerged arc welded (SAW) joints and gas metal arc welded (GMAW) joints. The simulation process and results were analyzed, and tensile force-displacement curves were generated. The findings indicate that during tensile loading, necking occurred in the base metal near the heat-affected zone (HAZ) for both welded joint models. After reaching tensile strength, the specimens fractured. These results suggest that the HAZ-adjacent base metal is a critical stress concentration region, and enhancing its tensile strength could effectively reduce pipeline cracking incidents, thereby improving service life.

Internal pressure load-bearing capacity experiments were performed on SAW and GMAW welded joints. The simulation process and results were analyzed, and Mises stress curves were plotted. The findings reveal that the welded joint region on the inner wall consistently experienced stress concentration throughout the loading process, eventually reaching the pressure-bearing limit. These results highlight that enhancing the compressive strength of the inner wall welded joint is essential for improving overall joint load-bearing performance.

### REFERENCES

- [1] Xia S, Zhang F, Yang Z. Cyclic deformation behaviours of 18Mn3Si2CrNiMo multiphase (martensite/bainite/retained austenite) steel[J]. Materials Science and Engineering A, 2019, 744: 64-73.
- [2] Bastola A, Wang J, Shitamoto H, et al. Investigation on the strain capacity of girth welds of X80 seamless pipes with defects[J]. Engineering Fracture Mechanics, 2017, 180: 348-365.

- [3] Chen X W, Qiao G Y, Han X L, et al. Effects of Mo, Cr and Nb on microstructure and mechanical properties of heat affected zone for Nb-bearing X80 pipeline steels[J]. *Materials & Design*, 2014, 53: 888-901.
- [4] Zheng Y, Zhang L, Shi Q, et al. Effects of hydrogen on the mechanical response of X80 pipeline steel subject to high strain rate tensile tests[J]. *Fatigue & Fracture of Engineering Materials & Structures*, 2020, 43(4): 684-697.
- [5] Li L, Yang Y H, Xu Z, et al. Fatigue crack growth law of API X80 pipeline steel under various stress ratios based on J-integral[J]. *Fatigue & Fracture of Engineering Materials & Structures*, 2014, 37(10): 1124-1135.
- [6] Zhao Z P, Qiao G Y, Lli G P, et al. Fatigue properties of ferrite/bainite dual-phase X80 pipeline steel welded joints[J]. *Science and Technology of Welding and Joining*, 2017, 22(3): 217-226.
- [7] Zhao Z P, Qiao G Y, Tang L, et al. Fatigue properties of X80 pipeline steels with ferrite/bainite dual-phase microstructure[J]. *Materials Science and Engineering A*, 2016, 657: 96-103.
- [8] Turichin G, Kuznetsov M, Pozdnyakov A, et al. Influence of heat input and preheating on the cooling rate, microstructure and mechanical properties at the hybrid laser-arc welding of API 5L X80 steel[J]. *Procedia CIRP*, 2018, 74: 748-751.
- [9] Xie Z Y, Qiao G Y, Zhao Z P, et al. STUDY ON FATIGUE PERFORMANCE OF WELDED HEAT-AFFECTED ZONE IN X80 STRAIN-BASED DESIGN PIPELINE STEEL [J]. *WELDED PIPE*, 2017, 40(05): 19-23.
- [10] Midawi A R H, Santos E B F, Huda N, et al. Microstructures and mechanical properties in two X80 weld metals produced using similar heat input[J]. *Journal of Materials Processing Technology*, 2015, 226: 272-279.
- [11] De Sousa L A, De Sousa L F G, Fonseca M C. Characterization of mechanical properties and residual stress in API 5L X80 steel welded joints[J]. *Journal of Materials Engineering and Performance*, 2018, 27(1): 124-137.
- [12] Kim Y, Kim C, Kim W, et al. Fatigue crack growth behavior for welded joint of x80 pipeline steel[C]. *Advanced Nondestructive Evaluation II*. 2009, 318-323.
- [13] Chen X W, Qiao G Y, Han X L, et al. Effects of Mo, Cr and Nb on microstructure and mechanical properties of heat affected zone for Nb bearing X80 pipeline steels[J]. *Materials and Design*, 2014 (53): 888-901.

### Author Profile

**Zhen Zhang** postgraduate student, School of Materials Science and Engineering, Xi'an Shiyou University.  
Research Direction: Metal Welding.